ELSEVIER

Journal of Organometallic Chemistry 512 (1996) 225–236

Journal of Organometallic Chemistry

ansa-Metallocene derivatives XXXII [1]. Zirconocene complexes with a spirosilane bridge: syntheses, crystal structures and properties as olefin polymerization catalysts [2]

Stefan Mansel, Ursula Rief, Marc-Heinrich Prosenc, Robin Kirsten, Hans-Herbert Brintzinger *

Fakultät für Chemie, Universität Konstanz, Postfach 5560, 78434 Konstanz, Germany

Received 31 July 1995; in revised form 8 November 1995

Abstract

Chiral *ansa*-zirconocene complexes with a trimethylene link between the Si bridge atom and an α-position of each C_5 ring ligand were prepared; two representatives, with i-propyl and t-butyl groups as β-substituents, were structurally characterized. The properties of these complexes with respect to MAO-activated propene polymerization were studied in comparison with those of their Me_2Si-bridged analogs. The t-butyl-substituted spirosilane complex gives a polymer with relatively high content of 3,1-insertions. These increased regioirregularities appear to be associated with decreased coordination gap aperture and increased lateral extension angles of the spirosilane-bridged zirconocene complexes; this notion is supported by a molecular-mechanics analysis of alternative olefin-insertion transition states.

Keywords: Zirconium; Aluminum; Polymerization; Metallocenes; Propene

1. Introduction

Chiral *ansa*-metallocenes have proved to be useful for a number of enantioselective catalysis reactions. Many contributions, especially with regard to structure-property relations for metallocene-catalyzed olefin polymerizations, have arisen from elegant work by Rausch and coworkers [1]. A particularly demanding goal, the development of stereoselective syntheses for racemic, C_2-symmetric *ansa*-metallocenes which avoid the formation of the achiral *meso*-isomer, was achieved by Rausch's synthesis of the spiro-germylene-bridged complex **1**. For this complex, the preferred formation of the racemic isomer was predicted by molecular-modelling studies, and indeed verified experimentally [2]. We have pursued the synthesis of spiro-bridged complexes of a different type, related to complexes of type **2**, which we have previously studied in our laboratory [3,4]. When the CH_3 substituents in α-position of the cyclopentadienyl ligands are connected to those at the silyl bridge by CH_2 units, to give complexes of general structure **3**, the necessarily C_2-symmetric spirosilane bridge and the steric requirements of the C_5-ring substituents will likewise favor the formation of the racemic product over that of a conceivable *meso*-like isomer. The close relationship between complexes of type **2** and **3** promises interesting insights into how the increased rigidity conferred on complexes **3** by the additional Si–Cp links affects their properties as polymerization catalysts.

2. Results and discussion

2.1. Syntheses and characterization of spirosilane-bridged zirconocene complexes

Ligand compounds **6a–d** were prepared as outlined in Scheme 1. 3-chloropropyl-3-bromopropyl-dichlorosilane (**4**), obtained by reaction of commercially avail-

* Corresponding author.

[1] For Part 31, see M.K. Leclerc and H.H. Brintzinger, *J. Am. Chem. Soc., 117* (1995) 1651.

[2] Dedicated to Professor Marvin D. Rausch on the occasion of his 65th birthday.

SSDI 0022-328X(95)06073-1

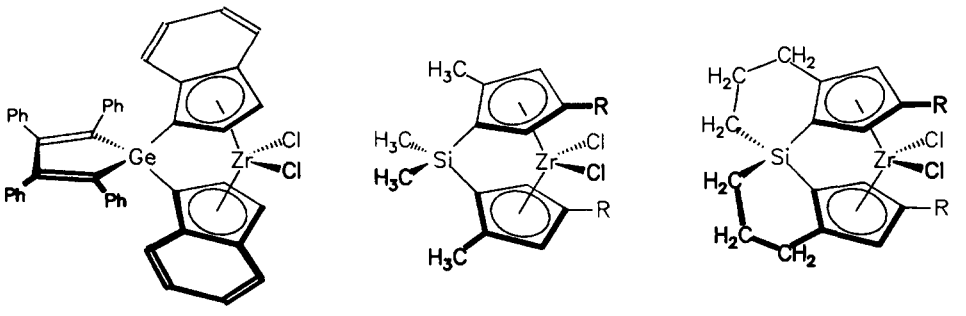

1 2 3

R: H (a), CH_3 (b), $CH(CH_3)_2$ (c), $C(CH_3)_3$ (d)

able 3-chloropropyl-trichlorosilane with allyl magnesium bromide [5] and subsequent photoinduced hydrobromination [6], was allowed to react with two equivalents of an appropriately substituted cyclopentadienide anion and the products **5a–d** cyclized by renewed aromatization (see Experimental Section). Compounds **6a–d** were obtained in the form of yellow oils or resins; their ^{1}H-NMR spectra show the broad resonances typical for silyl-substituted cyclopentadienes.

Reaction with two equivalents of n-butyl lithium in hexane at room temperature leads to an essentially complete precipitation of the respective dianionic lithium salts. As previously established for related reaction systems [7], a fast silatropic rearrangement generates an equilibrium mixture of neutral ligand isomers. Deprotonation of these is expected to give the anion with the sterically least encumbered silyl substituent.

Reaction of the ligand dilithium salts with $ZrCl_4$ in toluene gave product mixtures from which the desired spiro-bridged zirconocenes **3a**, **3c** and **3d** could be isolated in ca. 0.5–7% theoretical yield. In addition to the monomeric complexes, the crude product mixtures probably contain oligomeric reaction products, as indicated by mass spectra with $ZrCl_2$-containing fragment peaks at m/e values higher than those of the respective monomeric complex. ^{1}H-NMR spectra of the crude product mixtures indicate even lower fractions of monomeric products if the complexation is conducted in THF solution with $ZrCl_4 \cdot 2THF$. Complex **3a** was isolated from pentane solution, cooled to −80 °C, as a colorless precipitate. The β-methyl substituted complex **3b** could not be isolated. ^{1}H-NMR spectra of the product mixture indicate the presence of positional isomers. Apparently, the CH_3 substituents are sterically not demanding enough to direct the subsequent alkylation of the C_5 rings in an unequivocal manner.

Complexes **3c** and **3d** precipitated from their pentane solutions at −80 °C in the course of several weeks. Crystals of **3c** were obtained by slow evaporation of a THF solution at −24 °C in a glovebox. Slow evaporation of a THF solution at 4 °C in a normal atmosphere yielded crystals of complex **3d**, which is less sensitive to air and humidity.

The crystal structures of complexes **3c** and **3d**, represented in Fig. 1, show the expected axial symmetry. Their coordination geometry parameters (Table 1) are generally similar to those of **2d**. The structure of the spirosilane-bridged complex **3d** deviates from that of **2d**, however, in that the spirosilane rings pull the α-CH_2 substituent at each C_5 ring "backwards", in the direction of the bridge. Owing to the ensuing rotation of the C_5 rings, the β-substituents are placed in a more "forward" position, i.e. closer to the meridional centroid–Zr–centroid plane. The ^{1}H-NMR spectra of complexes

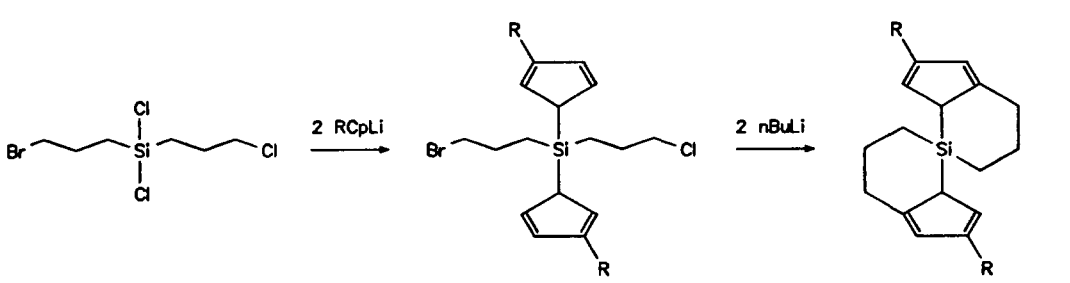

R: H (a), CH_3 (b), $CH(CH_3)_2$ (c), $C(CH_3)_3$ (d)

Scheme 1.

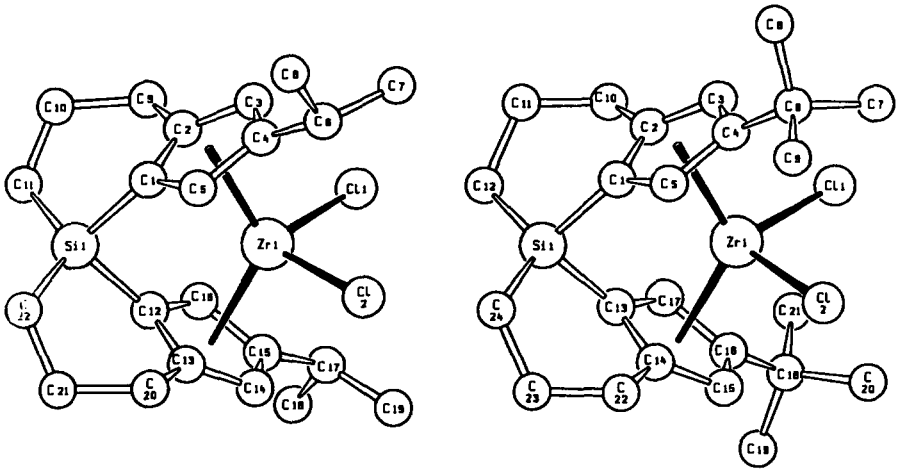

Fig. 1. Crystal structures of spirosilane-bridged complexes **3c** (left) and **3d** (right).

Table 1
Selected distances (pm) and angles (deg) for complexes **3c** and **3d**

3c		**3d**	
Zr(1)–Cl(1)	242.4(4)	Zr(1)–Cl(1)	242.7(3)
Zr(1)–Cl(2)	242.9(3)	Zr(1)–Cl(2)	243.1(5)
Zr(1)–C(1)	246.4(13)	Zr(1)–C(1)	244.1(15)
Zr(1)–C(2)	251.6(10)	Zr(1)–C(2)	251.7(16)
Zr(1)–C(3)	256.3(11)	Zr(1)–C(3)	257.6(14)
Zr(1)–C(4)	258.6(13)	Zr(1)–C(4)	260.6(11)
Zr(1)–C(5)	245.7(13)	Zr(1)–C(5)	247.0(12)
Zr(1)–C(12)	246.7(13)	Zr(1)–C(13)	246.9(12)
Zr(1)–C(13)	251.0(12)	Zr(1)–C(14)	250.3(10)
Zr(1)–C(14)	257.6(11)	Zr(1)–C(15)	260.4(11)
Zr(1)–C(15)	257.6(12)	Zr(1)–C(16)	264.4(10)
Zr(1)–C(16)	246.3(14)	Zr(1)–C(17)	247.8(9)
Cl(1)–Zr(1)–Cl(2)	99.1(1)	Cl(1)–Zr–Cl(2)	98.0(2)
CR(1)–Zr(1)–CR(2) [a]	126.6	CR(1)–Zr–CR(2) [a]	126.2
PL(1)–PL(2) [b]	61.1	Pl(1)–Pl(2) [b]	63.7
C(1)–Si(1)–C(12)	95.3(6)	C(1)–Si(1)–C(13)	94.3(3)
C(11)–Si(1)–C(22)	123.9(7)	C(12)–Si(1)C–(24)	122.8(8)

[a] CR(1) and CR(2) denote the centroids of lower and higher numbered C_5 rings respectively. [b] PL(1) and PL(2) denote the respective C_5-ring mean planes.

3c and **3d** (see Experimental Section) are in complete agreement with their solid state structures, that of **3a** agrees with the C_2-symmetric structure expected for this compound.

Alternative spirosilane-bridged ligands of type **9** were prepared, as outlined in Scheme 2, from diallyl-dichlorosilane by hydrosilylation with $HSiMe_2Cl$, introduction of two C_5-ring units and subsequent cyclization by reaction of the deprotonated C_5 rings with the remaining Si–Cl functions (see Experimental Section). The ^{1}H-NMR spectra of **9a** and **9b** indicate the presence of isomers with sp^3-bound H atoms as well as of isomers with two silyl groups at the same position of the C_5 ring. Deprotonation of a sample of **9b** with n-butyl lithium, subsequent hydrolysis and crystallization from a concentrated THF solution at 4 °C afforded crystals of compound **9b** suitable for a diffractometric structure determination. The molecular structure, represented in Fig. 2, establishes a triple-spiro structure with *ipso*-concatenated C_5 rings for this isomer of compound **9b**. A preference for *ipso*-positioned silyl groups has previ-

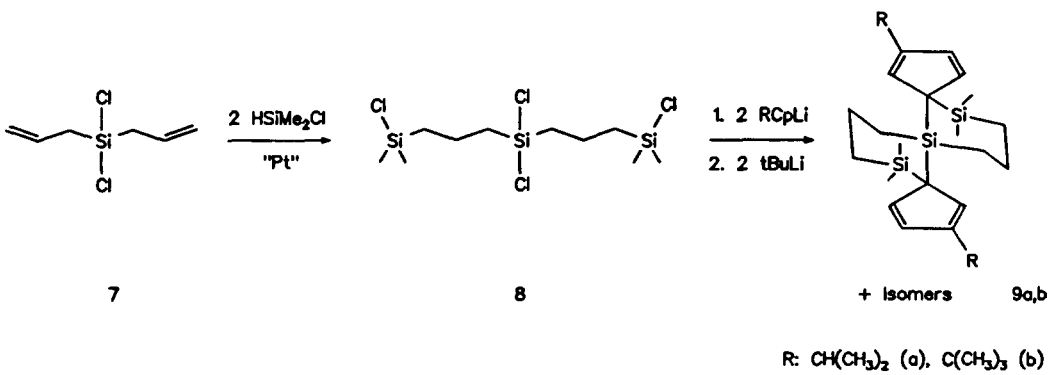

7 8

Scheme 2.

ously been reported by Jutzi [7] for a number of bis-silyl-substituted cyclopentadienyl compounds.

Compounds **9a** and **9b** are easily deprotonated by reaction with n-butyl lithium in diethyl ether. Reaction of the resulting dilithium salts with $ZrCl_4$ in toluene for two days at room temperature did not give any ^{1}H-NMR indications for the formation of monomeric zirconocene complexes. Instead, oligomeric products were apparently formed, as indicated by mass spectra with peaks at higher than expected m/e values.

The formation of the racemic complexes **3c** and **3d**, free from *meso*-like diastereomers, documents the principal validity of our approach. A serious drawback is revealed, however, by the low yields of these preparations and the failure of the dilithium salts of **9a** and **9b** to give any monomeric complexes with $ZrCl_4$. Apparently the spiro-bridged cyclopentadienide anions are preferentially attacked by $ZrCl_4$ from the outside, especially when shielded by sterically demanding substituents as in **9a** and **9b**, and are then prevented from intramolecular chelate formation by the fixed ligand geometry. Our observations would thus indicate that rotations of each C_5-ring moiety relative to the rest of the molecule are essential for an efficient formation of *ansa*-metallocene complexes from dilithiated ligand derivatives and a transition metal halide.

2.2. Propene polymerization catalysis

The properties of complexes **3a**, **3c** and **3d** as catalysts for the polymerization of propene were studied in reaction systems containing the respective complex, together with methyl aluminoxan (MAO, Al:Zr 1200:1) in toluene at 50 °C under a constant propene pressure of 2 bar (see Experimental Section). Productivities of these

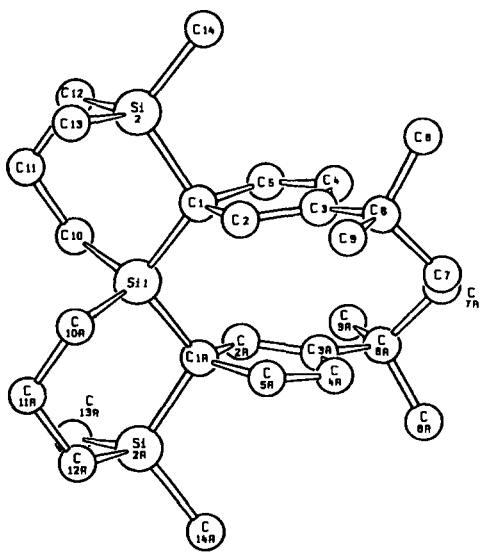

Fig. 2. Crystal structure of ligand **9b**.

Table 2
MAO-activated polypropene production with catalysts of type **2** and **3** (for reaction conditions see Experimental section)

Catalyst	**2c** [a]	**3c**	**2d** [a]	**3d**
Productivity [b]	14500	180	2100	1000
Melting point [°C]	130	138	149	128
M_w	13900	8400	12100	9800
M_w/M_n	1.74	1.37	1.62	1.75
Isotactivity [c]	82	90	99	97
3,1-Misinsertion [d]	< 0.5	< 0.5	0.7	2.5
Gap aperture [°] [e]	94	81	78	68
Lateral extension [°] [e]	167	185	167	187

[a] Values from Ref. [4]. [b] [kg(PP) per (h mol(Zr) bar)]. [c] [(%) mmmm pentads]. [d] In percent of all types of C_3H_6 unit (for determination see Experimental section). [e] See Fig. 3.

catalysts and properties of their polymer products are listed in Table 2, together with those of their Me_2Si-bridged analogs **2c** and **2d** [3,4]. Under the conditions used, **3a** produces a greasy polymer which was found to be essentially atactic ([mmmm] = 6%, M_W = 3700), even though complex **3a** is chiral in a formal sense. Previous studies have already established the importance of β-alkyl substituents for the stereospecifity of *ansa*-metallocene catalysts [3].

Complexes **3c** and **3d** gave isotactic polymers with [mmmm]-values of ca. 90 and 97% respectively (Table 2). That β-t-butyl-substituted homologs give increased stereoselectivities had also been observed for Me_2Si-bridged complexes [3,4]. Molecular weights are comparable for **2c** and **3c** and for **2d** and **3d** respectively. A notable difference between **3d** and its Me_2Si-bridged congener **2d** concerns the respective regioselectivities. While complexes **2c**, **2d** and **3c** give polypropenes with rather small frequencies (ca. 0.5%) of 3,1-insertions, we find ca. 2.5% of 3,1-inserted units in the polymer obtained with complex **3d** (Table 2). These misinserted units arise from a regioirregular, 2,1-oriented propene insertion when the ensuing secondary Zr–alkyl species rearranges to its terminally bound isomer before the next olefin inserts [8–10]. The melting points of the resulting polymers are significantly affected by these regioirregularities. The additional 2% of 3,1-inserted units generated by catalyst **3d**/MAO, as compared with **2d**/MAO, cause essentially the same melting point depression (ca. 20°) as the additional 3–4% of mrrm stereoerrors generated by catalyst **2c**/MAO.

The frequency with which an *ansa*-zirconocene catalyst introduces regioirregularities into a growing polymer chain appears to be related to the differing steric demands of the alternative olefin insertion transition states [11]. Since a secondary propene insertion places the CH_3 substituent of the olefin in a peripheral (rather than in a central) position, the transition state for such a secondary insertion is likely to require less space in the direction of the coordination gap aperture [12], but more

space in the lateral direction than a normal primary insertion. The data summarized in Table 2 do indeed indicate that a narrow gap aperture angle, together with a wide lateral extension angle (Fig. 3, cf. Appendix A) favors the occurrence of 2,1-insertions and, as a consequence, the incorporation of 3,1-units into the polymer.

This simplified graphical analysis is supported by results of more elaborate molecular-mechanics studies on the alternative transition states for primary and secondary propene insertions (cf. Appendix B). In the transition state for a 1,2-insertion, non-bonding repulsions of the β-C atom of the growing polymer chain with the β-t-butyl groups are stronger for **3d** than for **2d**, while for a 2,1-propene insertion the olefin CH_3 group interacts more strongly with the α-substituent of **2d** than with that of **3d**. This makes the difference in activation energies between secondary and primary insertions substantially smaller for complex **3d** than for **2d** (Fig. 4).

3. Experimental

All manipulations were conducted, unless noted otherwise, under exclusion of air and humidity in an inert gas atmosphere with Schlenk or glovebox techniques. Solvents were thoroughly dried by standard methods [10].

3.1. 3-Bromopropyl-3-chloropropyl-dichlorosilane (4)

Using a method described by Scott and Frisch [5], allyl-3-chloropropyldichlorosilane was obtained in 49% yield by reaction of 200 g (0.95 mol) of 3-

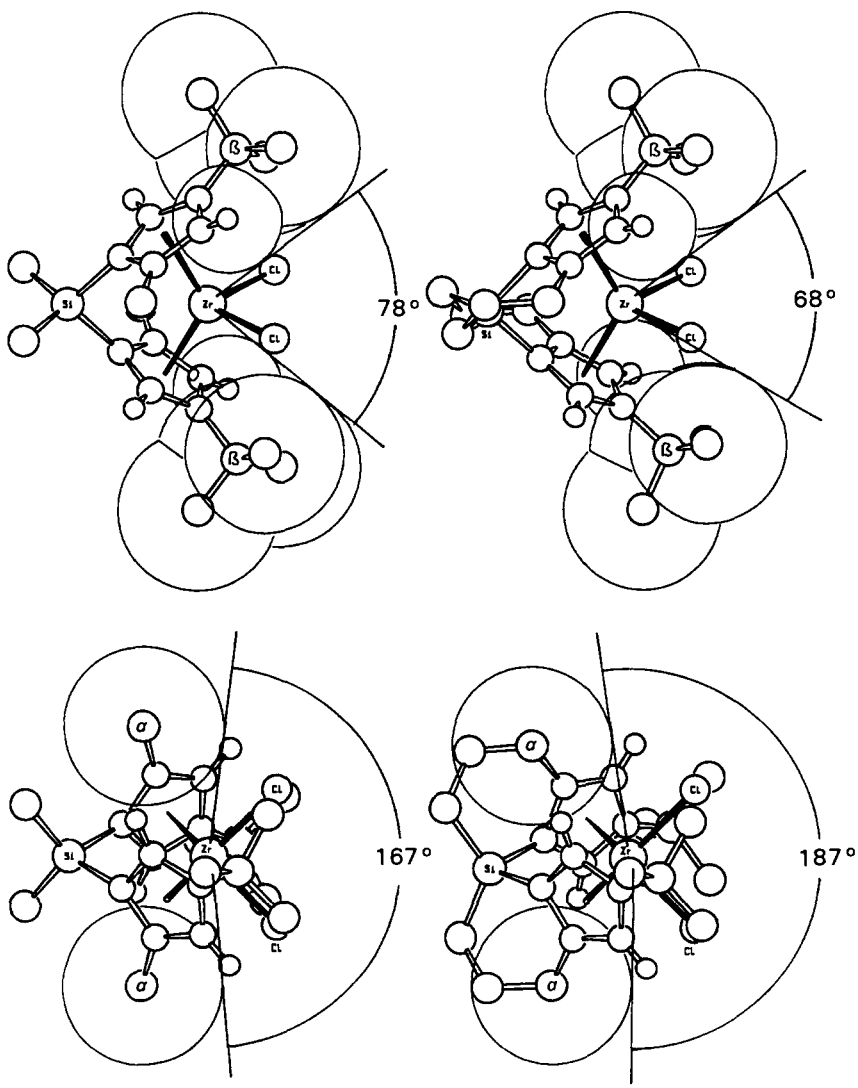

Fig. 3. Gap aperture (top) and lateral extension angles (bottom) for the Me_2Si-bridged complex **2d** (left) and the spirosilane-bridged complex **3d** (right, cf. Appendix A).

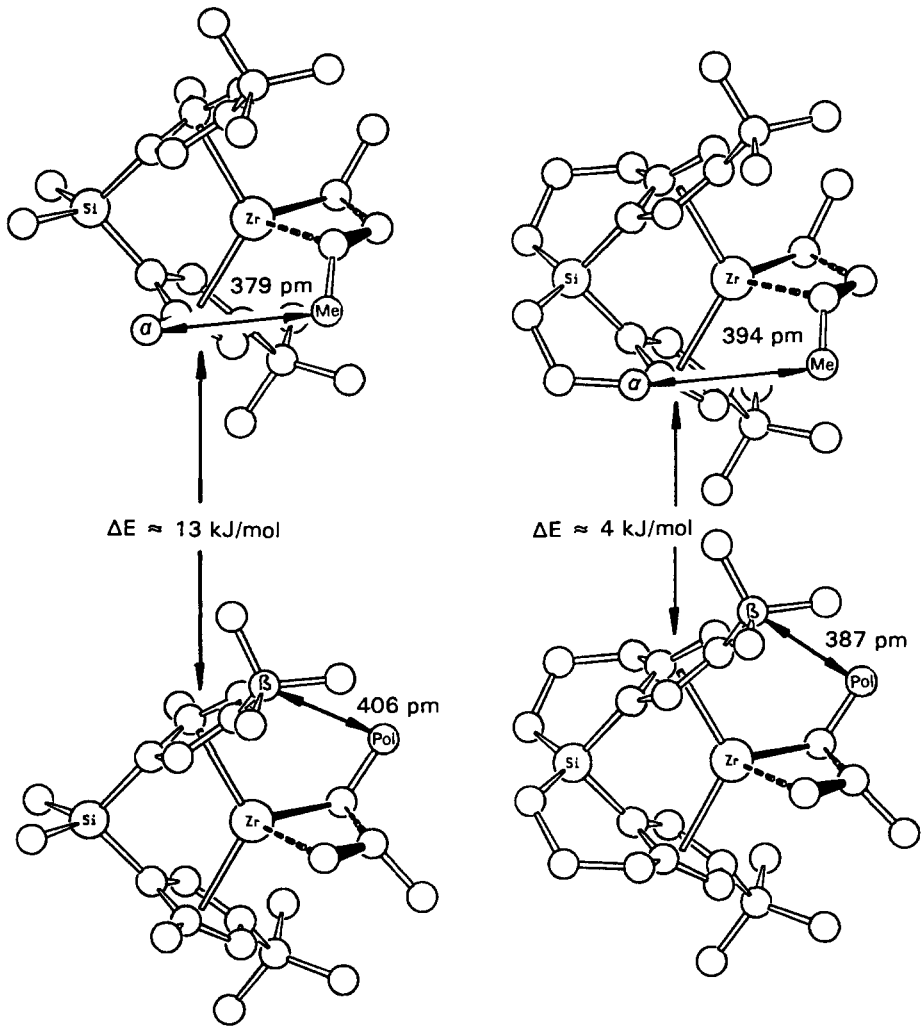

Fig. 4. Geometries and relative energies determined by a molecular-mechanics analysis for the transition states of a primary (1,2) insertion (bottom) and of a secondary (2,1) insertion (top) for cationic catalyst species derived from complex **2d** (left) and **3d** (right).

chloropropyl-trichlorosilane with 800 ml of a 1.06 M solution of allylmagnesiumbromid (0.85 mol) in diethyl ether. B.p. 94 °C (20 Torr). ^{1}H-NMR ($CDCl_3$, 250 MHz): δ 1.27 (m, 2H), 1.98 (m, 2H), 2.12 (td, 2H), 3.57 (t, 2H), 5.14 (m, 2H), 5.77 (m, 1H). MS (EI): m/z 177 ($M-C_3H_5^+$, 40%), 139 ($M-C_3H_6Cl^+$, 40%). A subsequent hydrobromation of 70 g (0.32 mol) of allyl-3-chloropropyl-dichlorosilane without solvent in a quartz vessel at 0 °C under intensive UV illumination by means of a mercury vapor lamp (Philips HPK 125W) led to the quantitative formation of 95.5 g of compound **4**. B.p. 85 °C (0.6 Torr). ^{1}H-NMR ($CDCl_3$, 250 MHz): δ 1.28 (m, 4H), 2.04 (m, 4H), 3.45 (t, 2H), 3.58 (t, 2H). MS (EI): m/z 221 ($M-C_3H_6Cl^+$, 80%), 177 ($M-C_3H_6Br^+$, 100%).

3.2. 3-Bromopropyl-3-chloropropyl-bis(cyclopentadienyl) silane (5a)

To 13.2 g (44 mmol) of 3-bromopropyl-3-chloropropyl-dichlorosilane (**4**) in 100 ml pentane and 60 ml THF were slowly added 6.3 g (88 mmol) of cyclopentadienyl lithium dissolved in 50 ml THF, whereupon a white precipitate was formed. After stirring for 1 h at room temperature, 200 ml of a saturated aqueous solution of ammonium chloride was added. The organic phase was separated, washed with 200 ml of deionized water and dried over magnesium sulfate. Removal of solvent in vacuo yielded 13 g of product **5a** (36 mmol, 82% of theoretical yield) as a yellow oil. ^{1}H-NMR ($CDCl_3$, 250 MHz): δ 0.45–1.05 (m, 4H), 1.82 (m, 4H), 3.05–3.58 (m, 2H), 3.35 (m, 2H), 3.42 (m, 2H), 6.50–6.96 (m, 8H). MS (EI): m/z 293 ($M-C_5H_5^+$, 10%), 237 ($BrSiCp_2^+$, 15%), 209 ($BrClSiCp^+$, 100%), 193 ($ClSiCp_2^+$, 20%).

3.3. 3-Bromopropyl-3-chloropropyl-bis(methylcyclopentadienyl) silane (5b)

To 7 g (23 mmol) of 3-bromopropyl-3-chloropropyldichlorosilane (**4**) in 25 ml pentane was slowly added 4 g (46 mmol) methylcyclopentadienyl lithium, dis-

solved in 50 ml THF. Stirring for one day at room temperature, aqueous work-up and removal of solvent in vacuo gave 6.5 g of compound **5b** (17 mmol, 73% of theoretical yield) as a yellow oil. ^{1}H-NMR ($CDCl_3$, 250 MHz): δ 0.4–1.0 (m, 4H), 1.65–2.0 (m, 4H), 2.0–2.15 (m, 6H), 2.94–3.03 (m, 2H), 3.28–3.6 (m, 4H), 6.05–6.8 (m, 6H). MS (EI): m/z 386 (M^+, 2%), 307 ($M-C_6H_7^+$, 10%), 265 ($M-C_9H_{13}^+$, 10%), 223 ($M-C_6H_7-(C_3H_6)_2^+$, 70%), 79 ($C_6H_7^+$, 100%).

3.4. 3-Bromopropyl-3-chloropropyl-bis(isopropylcyclopentadienyl) silane (5c)

To a solution of 4.46 g (15 mmol) of compound **4** in 30 ml THF and 120 ml pentane was slowly added 3.44 g (30 mmol) of isopropylcyclopentadienyl lithium, dissolved in 60 ml THF. After stirring for one day at room temperature, the yellow solution was decanted from the white precipitate and worked-up as described above. Removal of solvent from the product solution gave 4.8 g of compound **5c** (10.8 mmol, 72% of theoretical yield) as a yellow oil. ^{1}H-NMR ($CDCl_3$, 250 MHz): δ 0.42–1.0 (m, 4H), 1.17 (m, 12H), 1.52–2.0 (m, 4H), 2.72 (m, 2H), 2.94–3.01 (m, 2H), 3.26–3.54 (m, 4H), 6.10–6.83 (m, 6H). MS (EI): m/z 442 (M^+, 0.5%), 399 ($M-C_3H_7^+$, 0.5%), 335 ($M-C_8H_{11}^+$, 10%), 251 ($BrClSiC_8H_{11}^+$, 70%), 107 ($C_8H_{11}^+$, 100%).

3.5. 3-Bromopropyl-3-chloropropyl-bis(t-butylcyclopentadienyl) silane (5d)

17.2 g (58 mmol) of **4** in 150 ml pentane and 100 ml THF were allowed to react, at 0 °C, with 14.8 g (116 mmol) of t-butylcyclopentadienyl lithium, dissolved in 60 ml THF. The reaction mixture was stirred at room temperature overnight. Aqueous work-up and removal of solvent in vacuo gave 20.8 g (44 mmol, 76% of theoretical yield) of a yellow oil. ^{1}H-NMR ($CDCl_3$): δ 0.44–0.94 (m, 4H), 1.20 (s, 18H), 1.60–1.95 (m, 4H), 3,28 (m, 2H), 3,38 (m, 2H), 3,41 (m, 2H), 6.09 (bs, 2H), 6.50 (bs, 2H), 6.67 (bs, 2H). MS (EI): m/z 470 (M^+, 2%), 455 ($M-CH_3^+$, 0.5%), 413 ($M-C_4H_9^+$, 1%), 349 ($M-C_9H_{13}^+$, 30%), 263 ($BrClSiC_9H_{13}^+$, 100%).

3.6. Bis(cyclohexane-[b]-cyclopentadienyl) spirosilane (6a)

To a solution of 13 g (36 mmol) of 3-bromopropyl-3-chloropropylbis(cyclopentadienyl) silane (**5a**) in 350 ml THF was added at −50 °C, 46 ml of a 1.6 M solution (73 mmol) of n-butyl lithium in hexane. The reaction mixture was heated to reflux for 5 h. Aqueous work-up and removal of solvent in vacuo gave 8.35 g of compound **6a** (35 mmol, 96% of theoretical yield) as a viscous yellow oil. ^{1}H-NMR ($CDCl_3$): δ −0.10–2.50 (m, 12H), 2.70–3.50 (m, 2H), 5.90–7.10 (m, 6H). MS (EI): m/z 240 (M^+, 80%), 212 ($M-C_2H_4^+$, 35%), 133 ($M-C_8H_{11}^+$, 55%), 110 ($M-(C_5H_5)_2^+$, 100%).

3.7. Bis(cyclohexane-[b]-methylcyclopentadienyl) spirosilane (6b)

To 6.5 g (17 mmol) of 3-bromopropyl-3-chloropropyl-bis(methylcyclopentadienyl) silane (**5b**) dissolved in 50 ml pentane and 25 ml THF was added at −78 °C 21.5 ml of a 1.6 M solution (34 mmol) of n-butyl lithium in hexane. After adding another 20 ml THF and warming to room temperature, the reaction mixture became clear and was then heated for 4 h at reflux temperature. After aqueous work-up and removal of solvent in vacuo, 4 g (15 mmol, 87% of theoretical yield) of product **6b** remained as a yellow oil. ^{1}H-NMR ($CDCl_3$): broad signals in the aliphatic and olefinic regions. MS (EI): m/z 268 (M^+, 70%), 240 ($M-C_2H_4^+$, 35%), 149 ($M-C_9H_{11}^+$, 45%), 120 ($C_9H_{12}^+$, 50%), 71 ($HSiC_3H_6^+$, 100%).

3.8. Bis(cyclohexane-[b]-isopropylcyclopentadienyl) spirosilane (6c)

4.75 g (10.7 mmol) 3-bromopropyl-3-chloropropyl-bis(isopropylcyclopentadienyl) silane (**5c**), dissolved in 90 ml THF and cooled to −50 °C, was allowed to react with 13.5 ml of a 1.6 M solution (21.6 mmol) of n-butyl lithium in hexane. The reaction mixture was slowly warmed to room temperature and stirred for one day. Aqueous work-up of the yellow–red solution and removal of solvent in vacuo gave 3 g of compound **6c** (9.2 mmol, 86% of theoretical yield) as a yellow oil. ^{1}H-NMR ($CDCl_3$, 250 MHz): δ −0.05–2.50 (m, 12H), 1.19 (m, 12H), 2.83 (m, 2H), 2.5–3.55 (m, 2H), 5.62–6.75 (m, 4H). MS (EI): m/z 324 (M^+, 100%), 309 ($M-CH_3^+$, 20%), 281 ($M-C_3H_7^+$, 60%).

3.9. Bis(cyclohexane-[b]-t-butylcyclopentadienyl) spirosilane (6d)

An analogous reaction of 20.8 g (44.3 mmol) of 3-bromopropyl-3-chloropropyl-bis(t-butylcyclopentadienyl) silane (**5d**) in 200 ml pentane at 0 °C with 56 ml of a 1.6 M solution (89 mmol) of n-butyl lithium in hexane, addition of a further 90 ml of THF to dissolve the white precipitate after 2 h, and stirring for two days at room temperature gave, after work-up as described above, 15.5 g of **6d** (44 mmol, 99% of theoretical yield) as a yellow oil. ^{1}H-NMR ($CDCl_3$): δ −0.05–2.6 (m, 12H), 1.2 (m, 18H), 2.6–3.6 (m, 2H), 5.75–6.75 (m, 4H). MS (EI): m/z 352 (M^+, 1%), 337 ($M-CH_3^+$, 1%), 295 ($M-C_4H_9^+$, 1%), 231 ($M-C_9H_{13}^+$, 3%), 119 ($C_9H_{11}^+$, 55%).

3.10. Bis(spirosilacyclohexane-[b]-cyclopentadienyl) zirconium dichloride (3a)

The dilithium salt prepared from 2.2 g (9.1 mmol) of **6a** in 50 ml diethyl ether with 12 ml of a 1.6 M solution (19 mmol) of n-butyl lithium in hexane at −25 °C was collected by filtration under inert gas, washed with pentane and dried in vacuo to yield 2 g (7.9 mml, 87% of theoretical yield). This material was stirred with 1.9 g (8 mmol) of zirconium tetrachlorid in 200 ml toluene at 100 °C for 10 min. After cooling to room temperature and filtration, the reaction mixture was evaporated to dryness in vacuo and the residue extracted with 30 ml pentane. From this solution 20 mg (0.05 mmol, 0.5% of theoretical yield) of **3a** was obtained at −80 °C after several days as a colorless precipitate. MS (EI): m/z 400 (M^+, 40%), 362 ($M-HCl^+$, 100%). ^{1}H-NMR ($CDCl_3$, 250 MHz): δ 1.42 (m, 4H), 1.78 (m, 2H), 2.19–2.43 (m, 4H), 2.85 (m, 2H), 5.76 (t, 2H), 6.80 (m, 4H). No signals of any other zirconocene species are detectable in the ^{1}H-NMR spectrum.

3.11. Bis(spirosilacyclohexane-[b]-isopropylcyclopentadienyl) zirconium dichloride (3c)

To a solution of 3 g (9.2 mml) of **6c** in 50 ml pentane was added 11.5 ml of a 1.6 M solution (18.4 mmol) of n-butyl lithium in hexane. After stirring for two days the colorless precipitate was collected by filtration under inert gas, washed with a small volume of pentane and dried in vacuo. To 3.1 g (9.2 mmol, 100% of theoretical yield) of this dilithium salt were added 2.5 g (10.7 mmol) of $ZrCl_4$ and 200 ml of toluene. After stirring for two days at room temperature the brown suspension was evaporated to dryness in vacuo and the solid residue extracted with 100 ml of pentane. After cooling to −80 °C, 50 mg of complex **3c** was obtained as a light yellow precipitate (0.1 mmol, 1% of theoretical yield). MS (EI): m/z 484 (M^+, 40%), 446 ($M-HCl^+$, 100%). ^{1}H-NMR ($CDCl_3$, 250 MHz): δ 1.17 (d, 6H), 1.28 (d, 6H), 1.36 (m, 4H), 1.76 (m, 2H), 2.19 (m, 2), 2.25 (m, 2), 2.75 (m, 2), 3.16 (sp, 2), 5.30 (d, 2), 6.59 (d, 2H). The ^{1}H-NMR spectrum shows only signals due to complex **3c**; signals of other zirconocene species, in particular of positional isomers or oligomers, are not detectable.

3.12. Bis(spirosilacyclohexane-[b]-t-butylcyclopentadienyl) zirconium dichloride (3d)

The deprotonation of **6d** was conducted in analogy to the method described above for **6c**. To 2.9 g (7.7 mmol) of the dilithium salt of **6d** were added 1.8 g (7.7 mmol) of $ZrCl_4$ (freshly sublimed) and 150 ml of toluene and the mixture was stirred for 4 h at room temperature. The brown suspension was evaporated to dryness in vacuo and extracted with 60 ml of pentane. At 4 °C an oily precipitate was formed initially, which consisted of largely contaminated product. Cooling for several weeks to −80 °C gave 290 mg (0.56 mmol, 7% of theoretical yield) of **3d** as a yellow solid. MS (EI): m/z 512 (M^+, 70%), 497 ($M-CH_3^+$, 40%), 459 ($M-CH_3-HCl^+$, 75%). Anal. Found: C, 55.94; H, 6.63; Cl, 14.05. $C_{24}H_{34}Cl_2SiZr$ (512.75) Calc.: C, 56.22; H, 6.68; Cl, 13.83%. ^{1}H-NMR ($CDCl_3$, 250 MHz): δ 1.28 (m, 4H), 1.34 (s, 18H), 1.75 (m, 2H), 2.16 (m, 2H), 2.31 (m, 2H), 2.77 (m, 2H), 5.43 (d, 2H), 6.66 (d, 2H). ^{13}C-NMR ($CDCl_3$ 77.0 ppm, 250 MHz): δ 149.3, 137.2, 130.5, 109.4, 99.8, 33.7, 30.6, 28.4, 22.5, 8.7 ppm. The ^{1}H- and ^{13}C-NMR spectra show only signals due to complex **3d**; signals of other zirconocene species, in particular of positional isomers or oligomers, are not detectable.

3.13. Bis(4-chlorodimethylsilabutyl) dichlorosilane (8)

To a solution of 5.4 g (30 mmol) diallyldichlorosilane in 40 ml diethyl ether at 0 °C were added 10 mg of a Pt-catalyst (5% Pt on charcoal) and 6 g (64 mmol) dimethylchlorosilane. After stirring the reaction mixture for two days at room temperature, removal of solvent and volatile components in vacuo, 9.7 g (26 mmol, 87% of theoretical yield) of **8** were obtained as a colorless solid. ^{1}H-NMR ($CDCl_3$, 250 MHz): δ 0.42 (s, 12H), 0.94 (m, 4H), 1.20 (m, 4H), 1.60–1.70 (m, 4H). MS (EI): m/z 355 ($M-CH_3^+$, 7%), 235 ($M-C_5H_{12}ClSi^+$, 90%).

3.14. Bis(4-dimethyl-1,4-disilacycloheptan-[b]-i-propylcyclopentadienyl) spirosilane (9a)

To a solution of 4.4 g (12 mmol) of **8** in 80 ml THF and 100 ml pentane was added a solution of 2.7 g (24 mmol) isopropylcyclopentadienyl lithium in 20 ml THF. After stirring for two days at room temperature, the reaction mixture was cooled to −78 °C, treated with 15 ml of a 1.6 M solution of t-butyl lithium in pentane (24 mmol) and then slowly warmed to room temperature. Work-up with 100 ml of saturated aqueous ammonium chloride and subsequent washing with 50 ml of water gave 4.4 g (10 mmol, 83% of theoretical yield) of compound **9a**. ^{1}H-NMR ($CDCl_3$, 250 MHz): δ −0.6–0.4 (m, 12H), 0.5–2.3 (m, 12H), 1.13 (m, 12H), 2.72 (m, 2H), 2.9–3.3 (m, 2H), 6.0–6.7 (m, 4H). MS (EI): m/z 440 (M^+, 88%), 341 ($M-C_5H_{11}Si^+$, 35%), 333 ($M-C_8H_{11}^+$, 45%), 275 ($333-C_2H_6Si^+$, 95%). The dilithium salt was obtained by reaction of 4.4 g (10 mmol) of compound **9a**, dissolved in 50 ml of pentane, with 12.5 ml of a 1.6 M solution (20 mmol) of n-butyl lithium in hexane and collected by filtration. Drying in vacuo gave 3.6 g (8 mmol, 80% of theoretical yield) of the dilithium salt.

3.15. Bis(4-dimethyl-1,4-disilacycloheptan-[b]-t-butyl-cyclopentadienyl) spirosilane (9b)

Starting from 3.5 g (9 mmol) of **8**, 2.4 g (18 mmol) of t-butylcyclopentadienyl lithium and 11 ml of a 1.6 M solution (18 mmol) of t-butyl lithium in pentane, a reaction analogous to that described above for **9a** gave 3.7 g (8 mmol, 88% of theoretical yield of compound **9b**. ^{1}H-NMR ($CDCl_3$, 250 MHz): δ −0.45–0.40 (m, 12H), 0.5–2.2 (m, 12H), 1.17 (m, 18H), 2.9–3.2 (m, 2H), 5.9–6.8 (m, 4H). MS (EI): m/z 468 (M^+, 50%), 411 ($M-C_4H_9^+$, 10%), 349 ($M-C_9H_{11}^+$, 30%), 249 (349-$C_5H_{12}Si^+$, 25%). Anal. Found: C, 70.98; H, 10.27. $C_{28}H_{48}Si_3$ (468.96) Calc.: C, 71.72; H, 10.32%. Addition of 10 ml of a 1.6 M solution (16 mmol) of n-butyl lithium in hexane gave, after filtration and drying in vacuo, 2.18 g (4.5 mmol, 56% of theoretical yield) of the colorless dilithium salt. Hydrolysis of the filtrate with saturated aqueous ammonium chloride solution and partial evaporation of the organic phase gave, upon cooling to 4 °C, yellow crystals of compound **9b**, which were used for a diffractometric structure determination. These crystals gave the following ^{1}H-NMR ($CDCl_3$, 250 MHz): δ −0.75 (s, 6H), 0.04 (s, 6H), 0.5–2.2 (m, 12H), 1.16 (s, 18H), 5.90 (m, 4H), 6.22 (m, 2H).

3.16. Polymerizations and polymer analysis

Polymerizations were conducted in a 1 l autoclave (previously cleaned with a 0.5% solution of Al(i-butyl)$_3$ in toluene and dried in vacuo), using a solution of 6.25 μmol (ca. 3 mg) of each catalyst and 0.45 g of methylaluminoxane (Witco AG, molecular weight ca. 900), corresponding to an Al:Zr ratio of 1200:1, in toluene at 50 °C under a constant propene pressure of 2 bar. After a reaction time of 4 h, the reaction mixture was drained from the autoclave and stirred into a mixture of 1 l methanol and 10 ml concentrated aqueous HCl. The polymers thus precipitated were collected by filtration and dried at room temperature to constant weight. Molecular weight distributions were determined by GPC, melting points by DSC (Kunststoff-Labor, BASF AG).

Polymer ^{13}C-NMR spectra were measured in $C_2D_2Cl_4$ (δ 74.1 ppm) at 120 °C on a 250 MHz spectrometer operated at 62.9 MHz and analyzed with respect to stereo- and regioerror distributions according to methods described in the literature [11]. To determine the fraction of 3,1-misinsertions relative to all C_3H_6 units, the integrals of one of the 3,1-misinsertion signals at 20.73, 27.41 or 30.70 ppm was divided by 2 (because of the symmetry relation between the CH, CH_2 and

Table 3
Crystallographic data [a] for compounds **3c**, **3d** and **9b**

	3c	3d	9b
Formula	$C_{26}H_{38}Cl_2OSiZr$	$C_{24}H_{34}Cl_2SiZr$	$C_{28}H_{48}Si_3$
FW	556.8	512.7	468.9
Crystal color	yellow	yellow	yellow
Form	rhombohedral	rhombohedral	rhombohedral
Crystal system	monoclinic	monoclinic	monoclinic
Space group	$P2_1/n$	$C2/c$	$C2/c$
a (Å)	10.601(3)	26.673(6)	22.083(6)
b (Å)	17.960(5)	13.901(2)	9.841(4)
c (Å)	14.413(5)	19.737(5)	13.955(4)
β (deg)	104.93(3)	131.430(10)	105.06(2)
V (Å^3)	2651.6(14)	5486(2)	2928.7(17)
d_{calc} (g cm^{-3})	1.395	1.241	1.063
Z	4	8	4
Crystal size (mm^3)	0.2 × 0.1 × 0.1	0.3 × 0.3 × 0.3	0.3 × 0.3 × 0.2
Abs. coeff. (mm^{-1})	0.671	0.640	0.170
T (K)	243	247	296
Weighting scheme	$w^{-1} = \sigma^2(F) + 0.0002F^2$	$w^{-1} = \sigma^2(F) + 0.0006F^2$	$w^{-1} = \sigma^2(F) + 0.0002F^2$
Scan type	Wyckoff	Wyckoff	Wyckoff
Scan range (deg)	1.20	0.70	0.60
2θ Range (deg)	3.0 to 55.0	4.0 to 45.0	3.0 to 50.0
Scan speed (deg min^{-1})	1.50 to 14.65	2.00 to 29.30	2.30 to 29.30
Reflections collected	4678	7657	5651
Independent reflections	4395	3558	2585
Observed reflections	1870 ($F > 5.0\sigma(F)$)	2638 ($F > 4.0\sigma(F)$)	1704 ($F > 3.0\sigma(F)$)
No. of parameters	255	253	141
R_f [b]	6.89	6.23	5.82
R_{wf} [c]	6.16	9.21	5.07
Largest diff. peak (e Å^{-3})	0.58	1.74	0.35

[a] Conditions: Siemens R3m/V four-circle diffractometer, Mo Kα radiation (0.71073 Å), graphite monochromator. [b] $R_f = \Sigma(F_o - F_c)/\Sigma F_c$. [c] $R_{wf} = [\Sigma w(F_o - F_c)^2/\Sigma wF_o^2]^{1/2}$.

CH_3 groups which flank each 3,1-unit) and then related to the total integral between 20 and 22.5 ppm (which comprises CH_3 signals from all types of C_3H_6 unit, including those adjacent to 3,1-units as well as chain-end units). The ^{13}C-NMR spectrum of the polymer obtained with **3d**/MAO has a peculiar appearance: the CH_3 group adjacent to its 3,1-units and the following one give almost equally intense signals at 20.73 and 21.45 ppm. Since these chemical shifts are practically coincident with those of the (minimal) mmrm and mmmr pentad signals respectively, the spectrum closely resembles one which would arise from a chain-end controlled stereoerror distribution.

3.17. Crystal structure determinations

For crystals of complexes **3c** and **3d** and of ligand compound **9b**, obtained as described above, space group determinations, diffraction data collection and solution and refinement of the structures were conducted as summarized in Table 3. Complex **3c** crystallizes with one molecule of THF per asymmetric unit. Atom coordinates and thermal parameters for **3c**, **3d** and **9b** are listed in Tables 4–6.

Additional crystallographic data for compounds **3c**, **3d** and **9b** are available on request from Fachinforma-

Table 4
Atomic coordinates ($\times 10^4$) and equivalent isotropic displacement coefficients ($pm^2 \times 10^{-1}$) for complex **3c**

Atom	x	y	z	U_{eq} [a]
Zr(1)	1236(1)	1693(1)	4390(1)	28(1)
Cl(1)	2144(4)	1937(2)	3038(3)	57(1)
Cl(2)	1443(4)	345(2)	4449(3)	49(1)
Si(1)	106(4)	2877(2)	5729(3)	34(1)
C(1)	1772(12)	2516(6)	5805(10)	31(5)
C(2)	2055(12)	1795(6)	6186(8)	29(4)
C(3)	3148(13)	1535(7)	5883(9)	40(5)
C(4)	3567(14)	2073(8)	5333(11)	48(5)
C(5)	2690(14)	2676(7)	5246(10)	42(5)
C(6)	4733(17)	2040(11)	4936(15)	89(10)
C(7)	5719(21)	2584(11)	5398(19)	120(14)
C(8)	5301(20)	1309(12)	4942(19)	166(19)
C(9)	1341(13)	1443(7)	6853(9)	43(5)
C(10)	842(15)	2041(8)	7457(10)	51(6)
C(11)	−264(13)	2532(7)	6874(10)	45(5)
C(12)	−701(12)	2331(6)	4656(10)	27(4)
C(13)	−559(13)	2617(7)	3768(10)	33(5)
C(14)	−830(11)	2031(6)	3071(9)	32(4)
C(15)	−1151(13)	1391(7)	3520(9)	34(5)
C(16)	−1038(12)	1558(6)	4487(10)	35(5)
C(17)	−1613(14)	660(7)	3038(10)	42(5)
C(18)	−3115(14)	599(7)	2848(12)	58(7)
C(19)	−1258(16)	550(7)	2077(10)	54(6)
C(20)	−261(14)	3424(6)	3601(10)	44(5)
C(21)	−791(16)	3948(8)	4254(11)	59(6)
C(22)	−135(16)	3866(16)	5297(11)	52(6)
O(1)	1571(32)	−223(15)	606(18)	394(22)
C(51)	2549(26)	66(14)	1395(18)	174(11)
C(52)	3238(20)	−185(13)	2414(18)	187(12)
C(53)	2168(20)	−779(11)	2231(16)	119(7)
C(54)	1366(24)	−831(13)	1186(16)	162(10)

[a] Equivalent isotropic U defined as one-third of the trace of the orthogonalized U_{ij} tensor.

Table 5
Atomic coordinates ($\times 10^4$) and equivalent isotropic displacement coefficients ($pm^2 \times 10^{-1}$) for complex **3d**

Atom	x	y	z	U_{eq} [a]
Zr(1)	7192(1)	5983(1)	1271(1)	31(1)
Cl(1)	8044(2)	4744(2)	1949(2)	60(2)
Cl(2)	6890(2)	6059(2)	−191(2)	70(3)
Si(1)	6511(2)	7270(2)	1889(2)	38(2)
C(1)	6311(5)	6074(7)	1336(7)	34(7)
C(2)	6710(5)	5302(7)	1915(7)	33(7)
C(3)	6624(5)	4564(8)	1373(7)	40(8)
C(4)	6171(5)	4827(8)	456(7)	38(7)
C(5)	5989(5)	5778(7)	435(7)	39(7)
C(6)	5888(6)	4136(8)	−318(7)	50(8)
C(7)	6451(6)	3574(9)	−201(9)	62(11)
C(8)	5479(7)	3389(10)	−316(9)	70(11)
C(9)	5440(7)	4688(10)	−1222(8)	82(11)
C(10)	7082(6)	5308(8)	2903(7)	45(8)
C(11)	6739(7)	5879(9)	3134(9)	63(11)
C(12)	6715(6)	7004(9)	2970(8)	53(9)
C(13)	7266(5)	7457(7)	2031(7)	38(8)
C(14)	7139(5)	7782(7)	1242(7)	36(7)
C(15)	7710(5)	7613(7)	1349(7)	35(7)
C(16)	8204(5)	7207(7)	2196(7)	35(7)
C(17)	7920(5)	7055(7)	2602(7)	35(7)
C(18)	8924(5)	7069(9)	2630(8)	48(8)
C(19)	9236(6)	8062(9)	2902(9)	65(10)
C(20)	8968(6)	6627(10)	1955(9)	65(10)
C(21)	9321(6)	6382(10)	3452(8)	64(9)
C(22)	6501(5)	8322(8)	465(7)	46(8)
C(23)	6185(6)	8884(7)	761(8)	48(8)
C(24)	5915(5)	8248(8)	1099(8)	52(8)

[a] Equivalent isotropic U defined as one-third of the trace of the orthogonalized U_{ij} tensor.

Table 6
Atomic coordinates ($\times 10^4$) and equivalent isotropic displacement coefficients ($pm^2 \times 10^{-1}$) for **9b**

Atom	x	y	z	U_{eq} [a]
Si(1)	5000	695(2)	7500	29(1)
Si(2)	3581(1)	712(1)	7485(1)	41(1)
C(1)	4268(1)	1762(3)	7292(2)	30(1)
C(2)	4043(1)	2482(3)	6325(2)	31(1)
C(3)	3997(2)	3835(3)	6463(2)	32(1)
C(4)	4198(1)	4095(3)	7519(3)	36(1)
C(5)	4360(1)	2921(4)	8011(2)	35(1)
C(6)	3769(2)	4921(4)	5691(3)	39(1)
C(7)	4293(2)	5956(4)	5749(3)	63(2)
C(8)	3203(2)	5637(4)	5910(4)	61(2)
C(9)	3575(2)	4335(4)	4653(3)	57(2)
C(10)	5036(2)	−378(3)	8625(2)	40(1)
C(11)	4456(2)	−1226(4)	8621(3)	47(1)
C(12)	3881(2)	−356(4)	8622(3)	52(2)
C(13)	3265(2)	−428(4)	6403(3)	55(2)
C(14)	2944(2)	1861(4)	7638(3)	60(2)

[a] Equivalent isotropic U defined as one-third of the trace of the orthogonalized U_{ij} tensor.

tionszentrum Karlsruhe, D-76344 Eggenstein-Leopoldshafen 2, upon quotation of the depository number CSD-59125, the authors and the journal reference for this article.

Appendix A: Coordination gap aperture and lateral extension angles

The coordination gap aperture angle for a given *ansa*-metallocene complex defines the largest possible angle between two tangential planes which pass through the metal center and touch the inner van der Waals outline of the two β-substituents at each C_5-ring ligand [12]. It is calculated by an algorithm which requires the Cartesian position coordinates of the central metal, of the two ring centroids and the four β-substituents, as well as the van der Waals radii of the latter. The required atomic position coordinates can be taken from crystal structure determinations or from molecular modelling calculations. Structural data, e.g. for dichloro complexes with alkyl groups in β-position of their C_5 rings, will in general not give the largest possible gap aperture value unless the substituents are rotated about the C–C bonds connecting them with the C_5 ring so as to minimize their intrusion into the coordination gap. Equivalent results are obtained if the C atom connected to the C_5-ring is assigned an effective van der Waals radius of 1.9 Å for a methyl, 2.05 Å for an i-propyl and 2.5 Å for a t-butyl group. This simplified procedure certainly underestimates the effects of restrictions in rotational freedom on relative transition state energies.

The lateral coordination gap extension angle measures the restrictions which the α-substituents impose on the lateral extension of a reaction complex at the Zr center. It is determined as the angle between those two tangential planes which are perpendicular to the plane bisecting the coordination gap aperture angle, pass through the metal center and touch the inner van der Waals outline of the α-substituent closest to the bisector plane (in general the one opposite to the larger β-substituent at each ring). In complexes of type **2** and **3** it assumes values between 170 and 190° (Fig. 3). Entirely analogous geometrical parameters can be estimated for a putative transition-state complex involving e.g. alkyl and olefin ligands coordinated to a cationic Zr center. To assess the steric requirements for alternative olefin-insertion transition states, we use the geometries re-

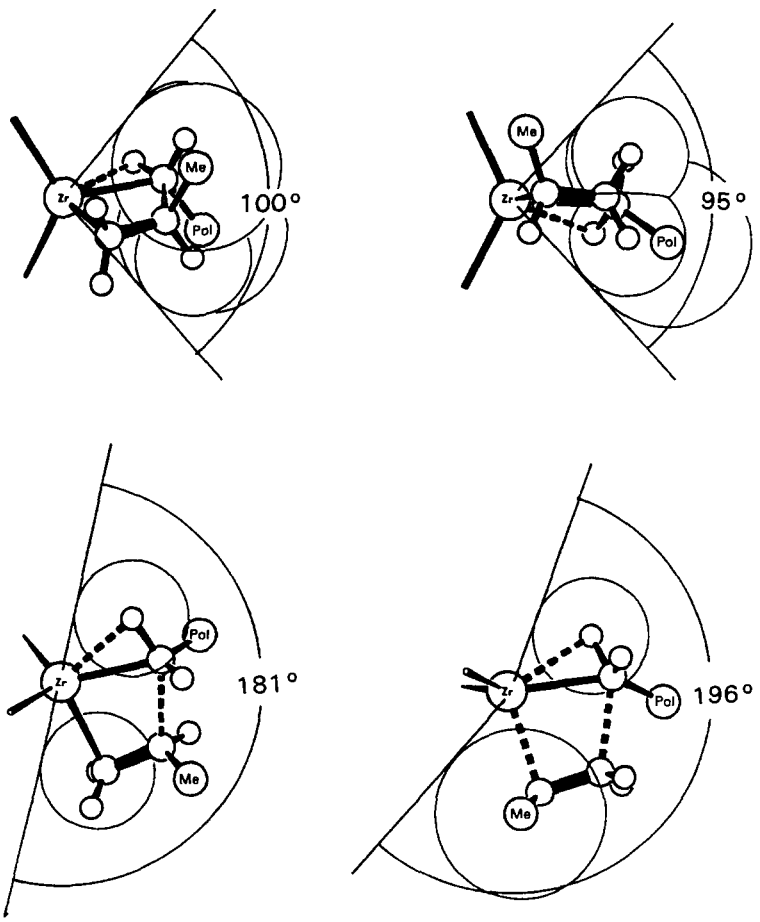

Fig. 5. Aperture (top) and lateral extension angles (bottom) for conceivable Zr-bound transition-state complexes for a primary (1,2) insertion (left) and for a secondary (2,1) insertion (right).

cently calculated for the Zr–C(α) · · · C(1)=C(2) skeleton of the cyclic olefin-insertion transition state by density functional methods [13] (Fig. 5, left). For the outer aperture angle of this 'reaction wedge', we determine a value of 100°, which is just somewhat larger than the aperture angles of the complexes considered above, especially of **3d**. This would indeed indicate some repulsive interactions for this reaction mode. For the outer lateral extension of this transition-state complex, we find — by an algorithm analogous to that described above for the inner lateral extension of the coordination gap — a value of 181°, which is just commensurate with the former.

For the transition state of a secondary olefin insertion, however, the lateral orientation of the CH_3 group of the olefin and the ensuing relaxed orientation of C(α)–C(β) chain-segment decrease the 'reaction-wedge' aperture to a value of ca. 95° (Fig. 5, right). This reaction mode would thus appear to avoid part of the steric pressure suffered by a primary insertion, especially with complex **3d**. The increased lateral extension of the secondary transition state is compatible, at the same time, only with the increased lateral gap extension of complex **3d** (Fig. 3), which is due to the 'backward' rotation of the C_5-ring ligands by the strained spirosilane bridge.

Appendix B: Molecular mechanics calculations

Relative energies of the alternative transition states for primary and secondary propene insertions have previously been studied in the groups of Corradini [14], Rappé [15] and Morokuma [16]. In the present study, the geometry of the four-membered, cyclic transition-state complex was assumed to be that determined by Ziegler and coworker [13] by local density methods and kept fixed as such, with the propene CH_3 group replacing one of the H atoms at one or the other of the olefin termini.

The relative energies of primary and secondary insertion-transition states are quite sensitive to the repulsion between the substituents at the incipient C · · · C bond. These repulsions tend to favor a secondary over a primary insertion. To obtain the opposite energy ordering, i.e. a lower activation energy for primary than for secondary insertions, rather small values had to be assigned to the angle and torsion force constants at the inner olefin terminus, while keeping those for the outer terminus at relatively high values (force constant listings are included in the supplementary material).

The geometries of the Zr-bound ligand frameworks, taken from the crystal structures of complexes **2d** and **3d**, were allowed to relax so as to meet the steric requirements of the Zr-bound transition-state complex by use of the molecular-mechanics program HYPERCHEM with a force field [17] which was modified so as to reproduce the crystallographically determined distortions of the ligand frameworks of *ansa*-zirconocene complexes of the type studied here [18].

Acknowledgements

Financial support of this work by BMFT, by BASF AG, by Fonds der Chemie and by funds of the University of Konstanz is gratefully acknowledged. We thank Dr. E. Keller, Kristallographisches Institut, Universität Freiburg, for providing the SCHAKAL-92 program package.

References

[1] R. Fierro, M.D. Rausch, G.S. Herrman and H.G. Alt, *J. Organomet. Chem., 485* (1995) 11; W.M. Tsai, M.D. Rausch and J.C.W. Chien, *Appl. Organomet. Chem., 7* (1993) 71; G. Hidalgo Llinas, S.H. Dong, D.T. Mallin, M.D. Rausch, Y.G. Lin, H.H. Winter and J.C.W. Chien, *Macromolecules, 25* (1992) 1242; D.T. Mallin, M.D. Rausch, Y.G. Lin, S. Dong and J.W.C. Chien, *J. Am. Chem. Soc., 112* (1990) 2030 and earlier references.

[2] Y.X. Chen, M.D. Rausch and J.C.W. Chien, *Organometallics, 13* (1994) 748.

[3] H. Wiesenfeldt, A. Reinmuth, E. Barsties, K. Evertz and H.H. Brintzinger, *J. Organomet. Chem., 369* (1989) 359; W. Röll, H.H. Brintzinger, B. Rieger and R. Zolk, *Angew. Chem., Int. Ed. Engl., 29* (1990) 279; B. Rieger, A. Reinmuth, W. Röll and H.H. Brintzinger, *J. Mol. Catal., 82* (1993) 67.

[4] A. Reinmuth, *Dissertation*, Universität Konstanz, 1992.

[5] R.E. Scott and K.C. Frisch, *J. Am. Chem. Soc., 73* (1951) 2599.

[6] J. Aretz, in E. Müller (ed.), *Houben-Weyl, Methoden der Organischen Chemie*, Vol. IV, No. 5a, Photochemie, 1975, part 1, p. 454; G. Kossmehl and A. Fluthwedel, *Chem. Ber., 122* (1989) 2413.

[7] P. Jutzi, *Chem. Rev., 86* (1986) 983.

[8] K. Soga, T. Shiono, S. Takemura and W. Kaminsky, *Makromol. Chem. Rapid Commun., 8* (1987) 305.

[9] A. Grassi, A. Zambelli, L. Resconi, E. Albizzati and R. Mazzocchi, *Macromolecules, 21* (1988) 617.

[10] B. Rieger and J.C.W. Chien, *Polym. Bull., 21* (1989) 159; B. Rieger, X. Mu, D.T. Mallin, M.D. Rausch and J.C.W. Chien, *Macromolecules, 23* (1990) 3559.

[11] H.H. Brintzinger, D. Fischer, R. Mülhaupt, B. Rieger and R. Waymouth, *Angew. Chem., Int. Ed. Engl., 34* (1995) 1143.

[12] K. Hortmann and H.H. Brintzinger, *New. J. Chem., 16* (1992) 51; P. Burger, K. Hortmann and H.H. Brintzinger, *Makromol. Chem. Macromol. Symp., 66* (1993) 127 (program available on diskette upon request).

[13] T.K. Woo, L. Fan and T. Ziegler, *Organometallics, 13* (1994) 2252.

[14] L. Cavallo, P. Corradini, G. Guerra and M. Vacatello, *Polymer, 32* (1991) 1329; G. Guerra, L. Cavallo, G. Moscardi, M. Vacatello and P. Corradini, *J. Am. Chem. Soc., 116* (1994) 2988.

[15] L.A. Castonguay and A.K. Rappé, *J. Am. Chem. Soc., 114* (1992) 5832.

[16] H. Kawamura-Kuribayashi, N. Koga and K. Morokuma, *J. Am. Chem. Soc., 114* (1992) 8687.

[17] T.N. Doman, T.K. Hollis and B. Bosnich, *J. Am. Chem. Soc., 117* (1995) 1352.

[18] M.H. Prosenc and H.H. Brintzinger, in preparation.